Shear-Induced Crystallization in Novel Long Chain Branched Polypropylenes by in Situ Rheo-SAXS and -WAXD

Pawan K. Agarwal,*,† Rajesh H. Somani,‡ Weiqing Weng,† Aspy Mehta,† Ling Yang,‡ Shaofeng Ran,‡ Lizhi Liu,‡ and Benjamin S. Hsiao*,‡

Baytown Polymers Center, ExxonMobil Chemical Company, Baytown, Texas 77522, and Department of Chemistry, State University of New York, Stony Brook, New York 11794-3400

Received February 5, 2003; Revised Manuscript Received May 1, 2003

ABSTRACT: The characteristic properties of a new class of long chain branched isotactic polypropylene (LCB-iPP) polymers and the effects of its molecular architecture on the nature of orientation-induced crystallization precursor structures and crystallization kinetics in flow were investigated. In these polymers, long chain branching (LCB) was introduced via in situ polymerization of propylene and a diene monomer using the metallocene catalyst technology. The LCB-iPP polymers exhibited improved melt strength and mechanical properties, such as flexural modulus and tensile yield strength. As determined by gel permeation chromatography coupled with multiangle laser light-scattering (GPC−MALLS) analysis, it was noted that the LCB-iPP polymers had a significant population of highly branched chains in the high molecular weight component of the molecular weight distribution. Dynamic viscoelastic properties obtained by small-amplitude oscillatory shear technique showed that the increase in the degree of LCB caused a broadening of the melt relaxation spectrum, especially in the longest relaxation time regime. The effects of the unique molecular architecture of the LCB-iPP polymers on shear-induced crystallization development was investigated by in situ rheo-SAXS (small-angle X-ray scattering) and -WAXD (wide-angle X-ray diffraction) techniques. The results showed that upon application of a step shear (rate = 60 s^{-1}, t_s = 0.25 s, T = 140 °C), the oriented crystals fraction was substantially higher in the LCB-iPP polymers than that in the linear iPP polymer. The shear-induced crystallization rate of the LCB-iPP polymers was analyzed by an Avrami model; the value of Avrami exponent, n, ranged from 1.8 to 2.8 indicating a rod or disklike crystal growth geometry. In addition, the crystallization kinetics was enhanced by more than an order of magnitude when compared to linear iPP polymer under shear. The details of the crystalline phases determined from the WAXD data showed that, in addition to monoclinic α-form crystals, they were triclinic γ-form crystals. The contribution of γ-form crystals to the total crystalline phase was independent of the LCB level and was attributed to the regio defects of the chain. Enhancements in various mechanical properties as well as their strong crystal orientation and improved crystallization kinetics in flow, are due to the unique molecular architecture of these LCB-iPP polymers, which in turn are strongly coupled to their broadened and complex relaxation behavior.

Introduction

Processing and shaping operations of semicrystalline polymer materials, such as extrusion, injection molding, fiber spinning, etc., cause orientation and crystallization of polymer molecules in the melt, which strongly influences the final polymer morphology such as spherulitic, shish/kebab, and row-nucleated, etc.[1−20] In isotactic polypropylene (iPP), the flow-induced morphology, characteristic features of the crystalline phase, (i.e., relative quantities of the oriented and unoriented crystals), and its nature (crystal form, α, β, or γ) in the final product has a direct effect on the product properties and performance. In visualizing the effects of flow on the orientation and structural evolution, one needs to be cognizant of some key fundamental characteristics of the polymers. These include the polymer molecule architecture such as the chain rigidity, interchain friction (or viscosity), chain branching, chain length and its distribution, as well as the efficiency of the orientation of the chains under given flow kinematics: shear, elongational or mixed.

* To whom correspondence should be addressed. E-mail addresses: P.K.A., pawaalka@hotmail.com; B.S.H., bhsiao@notes.cc.sunysb.edu.
† ExxonMobil Chemical Co.
‡ State University of New York, Stony Brook.

Recently, through the utilization of the metallocene catalyst technology, many structural features, including long chain branching (LCB), can be introduced into polymer chains during polymerization.[21−23] For example, Markel et al.[24] reported on the synthesis of LCB polyethylene (PE) block copolymers through incorporation of the in situ generated vinyl-terminated, crystallizable macromonomers. The properties of comblike polymers depended on the catalyst pair and the process conditions selected. The later determined the topological details of the branched polymer as well as the LCB distribution. GPC−FTIR analysis of model polymers with different LCB and backbone compositions revealed their LCB distribution pattern with the highest molecular weight molecules containing the highest levels of branching. Also, Weng et al.[25−27] prepared LCB isotactic polypropylene polymers by the incorporation of preformed iPP macromonomers (or oligomers) having predominantly vinyl-terminated chain ends in size ranges above the M_e, the entanglement molecular weight for iPP. These LCB-iPP polymers exhibited improved melt properties, such as strain hardening and shear thinning.

Similar to the above approach, a new class of LCB-iPP polymers, in which LCB was introduced via in situ polymerization of propylene and a diene monomer, were prepared using metallocene catalyst technology.[28] These polymers exhibit some atypical characteristics. For

10.1021/ma034154l CCC: $25.00
Published on Web 06/10/2003

Table 1. Composition, Thermal Properties, and Molecular Weights of the LCB-iPP Polymers[a]

sample	diene level (ppm)	mol wt M_n	M_w	M_z	M_{z+1}	T_m (°C)	T_c[b] (°C)
LCB 01	0	51 000	150 000	249 000	356 000	152.2	112.9
LCB 05	170	52 000	203 000	460 000	845 000	153.9	122.2
LCB 07	250	66 000	229 000	527 000	949 000	154.6	124.4
LCB 13	375	112 000	276 000	634 000	1 118 000	154.3	125.2

[a] T_m and T_c were obtained by DSC at a heating/cooling rate of 10 °C/min. The molecular weights were determined by GPC [b] Crystallization temperature determined during cooling.

example, a unique molecular weight dependence on the diene concentration is noted. The number-average molecular weight, M_n, remains relatively constant, while the high molecular weight components, M_w, M_z, M_{z+1}, increased significantly with the diene level. Thus, the highly branched species reside at the high molecular weight species of the molecular weight distribution. Second, a broadening of the melt relaxation spectrum with increasing level of diene concentration is observed. In the first part of this paper, we present some of the characteristic properties of these novel LCB-iPP polymers.

The unique molecular architecture of these LCB-iPP polymers provides an opportunity to study its effects on the flow-induced orientation and structure developments that are critical in many polymer fabrication processes, such as thermoforming, foaming, and blow molding, etc. In flow-induced crystallization,[29−45] it is generally accepted that orientation of polymer molecules in flow direction promotes alignments and interactions of chains. The net result is an increase in the number of nuclei and crystallization kinetics. There are a few reports[46] of the effects of molecular weight on flow-induced crystallization of linear polymers. However, to our knowledge, the effects of the long chain branching (LCB) in polypropylene polymers have not been reported so far. For a given polymer molecular weight, the LCB is expected to affect the relaxation behavior of molecules in the melt, and in turn the morphological features of the crystallized polymer. In situ rheo-SAXS and -WAXD techniques are used to evaluate the effects of the LCB on the development of the shear-induced crystallization precursor structure, the nature of crystalline phases and the crystallization kinetics of these polymers. The results of X-ray studies are presented in the second part of this paper.

Experimental Section

Materials. The LCB-iPP polymers were prepared on a pilot scale, following a proprietary process.[28] The polymers were made with varying levels of diene charged to reactor. Controlled and desired M_w, MWD, and melt flow rate (MFR) of the polymer was achieved. The granular polymer products were used as such or in their pellet forms that contained a conventional PP stabilizer package. The composition of the four samples selected for detailed characterization and in situ rheo-SAXS and -WAXD studies are shown in Table 1. The linear iPP polymer sample (LCB 01), was prepared under the same reaction conditions as the diene modified LCB-iPP polymers except that no diene was added during its synthesis.

Characterization of LCB-iPP Polymers. Molecular weight characteristics were determined using a Waters 150C high-temperature gel permeation chromatograph (GPC) operating at 135 °C. Melting and crystallization temperatures were measured on a TA Instrument DSC-912 using a heating or cooling rate of 10 °C/min. The melting temperatures reported were obtained from the second melting endotherm.

The light-scattering experiments were conducted using an instrument combining multiangle laser light scattering with a Waters 150C gel permeation chromatograph (GPC−MALLS, made by Wyatt Technology, Inc.). This instrument allowed the measurement of polymer molecular weight and radius of gyration. The MALLS detector contained a 30 mW argon ion laser and an array of photodiodes. The photodetectors were calibrated with NBS1482, a polyethylene standard with a stated molecular weight of 13 600 and polydispersity of ∼1.2. A radius of gyration, R_g, value of 5 nm was assumed for this polymer.

Dynamic viscoelastic properties were determined from small amplitude oscillatory shear measurements using a parallel plate rotational rheometer, RMS800 (Rheometrics Scientific). The extensional viscosity data were obtained using a Rheometrics melt elongational rheometer (RME) in an extensional strain mode at 160 °C. The elongation rates were determined by an image analysis procedure that is believed to be more accurate than the command value on the instrument. The granular polymers were stabilized with 0.1−0.2 wt % of BHT (2,6-di-*tert*-butyl-4-methylphenol) and molded into rectangular test specimens 60 × 8 × 2 mm^3 prior to tests.

Mechanical properties of LCB-iPP polymers were measured following the standard American Society of Testing Materials (ASTM) type test procedures. The polymers were injection molded on a 75 Ton Van Dom injection press (model # 75-RS-3F), to make ASTM test specimen for flexural modulus, yield strength, and heat distortion temperature measurements. A straight extrusion temperature profile of 240 °C, injection pressure of 600 psi, and mold temperature of 60 °C were used for molding.

In Situ Rheo-SAXS and -WAXD. In situ rheo-SAXS and -WAXD measurements were carried out in the synchrotron X-ray beamline X3A2 at the National Synchrotron Light Source (NSLS), Brookhaven National Laboratory (BNL). A 2D MAR CCD X-ray detector (MARUSA) having a resolution of 1024 × 1024 pixels (pixel size = 158.44 μm) was employed to detect time-resolved SAXS and WAXD patterns in the shear experiments. The sample to detector distance for SAXS and WAXD was 1165 and 98.5 mm, respectively. The data acquisition time for each scattering pattern (image) was 10 s, with an interval of 5 s between adjacent images. Typically 120 images were collected in a single run.

In each experiment, the polymer sample in the form of a ring, cut from the compression-molded, 0.5−1.0 mm thick films, was mounted between the two X-ray windows (diamond and Kapton film) in the Linkam shear stage. The gap between the two windows was adjusted to the sample thickness. All samples were subjected to nearly identical thermal history and believed to be free of memory effects. The temperature control program for the shear stage was as follows:

(a) Heat the polymer sample from room temperature to 200 °C at a rate of 30 °C/min.

(b) Keep the polymer melt by holding the temperature at 200 °C for 5 min.

(c) Cool at a rate of 30 °C/min down to 140 °C.

(d) During X-ray measurements, hold the temperature at 140 °C.

Polymer melt was subjected to shear immediately after its temperature reached 140 °C. The chosen shear mode was a step-shear: shear rate of 60 s^{-1} and strain of 1430%. This corresponds to a shear duration of $t_s = 0.25$ s. Two-dimensional patterns (SAXS or WAXD) were collected continuously; that is, before, during, and after cessation of the applied shear. The details of the experimental procedures for rheo-SAXS and -WAXD experiments have been described elsewhere.[47−49]

Results

Molecular Characteristics of LCB-iPP Polymers. Molecular Weights and Melting Behavior. Table 1 shows the molecular weights, M_n, M_w, M_z, and M_{z+1}, measured by GPC and nominal melting point (T_m) and crystallization temperatures (T_c) obtained by DSC of

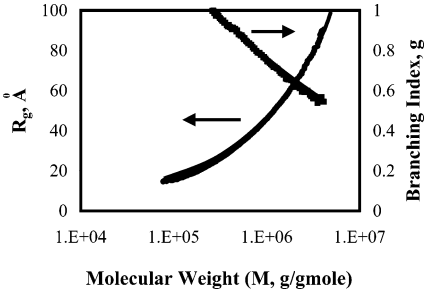

Figure 1. Radius of gyration and branching index of LCB 07 polymer sample.

various LCB-iPP polymers of the present study. It is noted that the number-average molecular weight for samples LCB 01, 05, and 07 remain relatively constant, while the higher molecular weight components (M_w, M_z, and M_{z+1}) increase significantly with increasing diene level. This is a unique feature of these LCB-iPP polymers. Note that since all the LCB-iPP samples have similar T_m and T_c values, the samples are subjected to an identical degree of subcooling at the test temperature of 140 °C. Consequently, the results of rheo-SAXS and -WAXD studies for different polymer samples can be compared directly to evaluate the effects of LCB on the shear-induced crystallization development.

GPC—MALLS Analysis to Characterize LCB-iPP. The polymer molecular weight (M, absolute value) and radius of gyration (R_g) of polymer fractions from GPC columns were measured by the GPC−MALLS instrument. The absolute molecular weight was determined by light scattering at each retention volume, and the R_g value of the polymer was obtained by fitting the angular dependence of the light-scattering signal to a random coil model (both linear and branched molecules).[25] The branching index (g) can be defined as follows:

$$g = R_{g,branched}{}^2/R_{g,linear}{}^2 \quad (1)$$

$R_{g,branched}$ and $R_{g,linear}$ are the radii of gyration of branched and linear polymers of equivalent molecular weight. Thus, a value smaller than 1 indicates branching. The lower the branching index, the higher the branching level. Figure 1 shows the R_g and g values as a function of the molecular weight for LCB 07 sample; a similar trend is observed for the other samples. It is seen in Figure 1 that the higher molecular weight species have a lower branching index, i.e., a higher degree of branching. A similar behavior was observed for the other branched polymers. From these results and molecular weights in Table 1, it can be concluded that in these LCB-iPP polymers *the highly branched species reside at the high molecular weight (long chain) species of the molecular weight distribution (MWD).* This is an important factor in the flow-induced crystallization development. The high molecular weight species in the molecular weight distribution have the strongest effect on the formation of polymer nuclei due to their underlying relaxation behavior.

A weight-average branching index, $g_{\langle w\rangle}$, as defined in eq 2, may be used for comparison of the branching level in LCB-iPP samples

$$g_{\langle w\rangle} = \frac{\sum C_i R_{gi}{}^2}{\sum C_i (K M_i{}^{\alpha})^2} \quad (2)$$

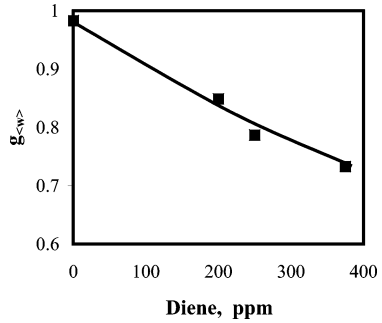

Figure 2. Effect of diene level in LCB-iPP polymers on the weight-average branching index.

where C_i and R_{gi} are the concentration and radius of gyration of the ith species, and K and α are the coefficient and exponent of the fitted curve (power law) for R_g vs molecular weight (M) data for the corresponding linear polymer. Figure 2 shows the calculated weight-average branching index ($g_{\langle w\rangle}$) values for the LCB-iPP samples as a function of diene level. It is seen that the branching index of LCB-iPP polymers decreased as the diene concentration is increased.

Melt Rheology. Relaxation Behavior. In a small amplitude oscillatory shear experiment, the dynamic moduli are expressed as in-phase (G') and out-of-phase (G'') components of the sinusoidal stress, τ

$$\tau = \tau_o \sin(\omega t + \delta) = G'\gamma_o \sin \omega t + G'' \gamma_o \cos \omega t \quad (3)$$

where γ_o is the amplitude of the imposed strain, ω is the angular frequency, and δ is the phase angle between strain and stress. The complex motion of polymer chains in the melt is described by a set of different relaxation modes in terms of a relaxation time spectrum. Mathematically, it is expressed as a discrete set of exponential decays, which constitute the relaxation modulus, $G(t)$, as given below.

$$G(t) = G_e + \sum_{i=1}^{N} g_i e^{-t/\lambda_i} \quad (4)$$

where N is the number of relaxation modes, λ_i is relaxation time of the ith mode and g_i is the strength of the ith mode. The equilibrium modulus G_e is finite for solids ($G_e > 0$) and zero for liquids ($G_e = 0$).

The dynamic moduli G' and G'' can also be expressed in terms of the relaxation time spectrum, but in frequency domain as in eqs 5 and 6.

$$G'(\omega) = G_e + \sum_{i=1}^{N} g_i \frac{(\omega\lambda_i)^2}{1 + (\omega\lambda_i)^2} \quad (5)$$

$$G''(\omega) = \sum_{i=1}^{N} g_i \frac{\omega\lambda_i}{1 + (\omega\lambda_i)^2} \quad (6)$$

Thus, from eqs 4−6, the discrete relaxation spectrum can be determined from the experimental dynamic moduli data. The method of Baumgartel and Winter[50] using the Iris software (available from Rheometrics) was applied to determine parameters of the discrete relaxation spectrum by fitting eqs 5 and 6 to G' and G'' data. The coefficients g_i and relaxation times λ_i were determined such that the average square deviation between predicted G' and G'' values and measured G' and G''

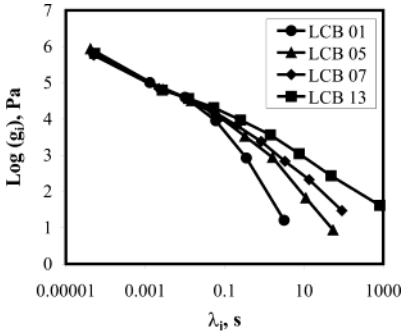

Figure 3. Relaxation behavior of the LCB-iPP polymer melts at 180 °C.

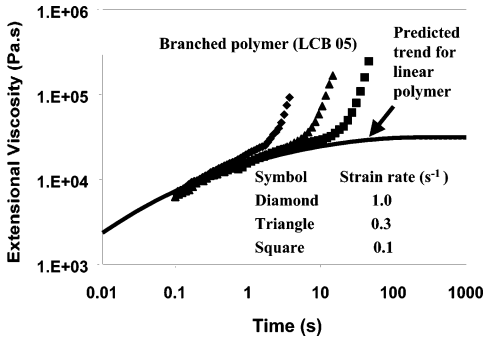

Figure 4. Extensional viscosity growth curve for LCB-iPP polymers (LCB 05) and linear polymer. (Extensional viscosity values for linear polymer were predicted from shear viscosity data.)

data is minimum. The nonlinear regression simultaneously adjusted not only g_i and λ_i parameters but also the number of relaxation times N during the iterative calculations to obtain a best fit of G' and G'' experimental data.

The calculated values of the discrete relaxation spectrum are presented in Figure 3. Figure 3 shows that the shortest relaxation modes are dominating for all the four samples; however the increase in the diene level in LCB-iPP resins results in broadening of the relaxation spectrum in the longest relaxation time regime. The sample with 375 ppm of diene (LCB 13) shows the broadest relaxation spectrum.

Extensional Viscosity and Strain Hardening. In an elongational viscosity vs time plot for a polymer, typically the strain hardening phenomenon is implied by an abrupt upswing away from the predicted behavior of a linear viscoelastic material. Strain-hardening is, generally, attributed to the presence of long chain branches in polymer.[51] The extent of strain hardening of polymer melt at a given strain rate can be obtained from ratio of the extensional viscosity to the linear viscosity at the break point. Figure 4 shows a typical extensional viscosity growth curve for LCB-iPP (LCB 05). For comparison, the predicted values of the extensional viscosity for the corresponding linear polymer are also shown in Figure 4. The transient elongational viscosity, $\bar{\eta}_e(t)$, for the linear polymer (3 times the shear viscosity) was obtained from the dynamic data using eq 7.

$$\bar{\eta}_e(t) = 3\sum_{i=1}^{N} g_i\lambda_i(1 - e^{-t/\lambda_i}) \qquad (7)$$

As seen in Figure 4, extensional viscosity for the linear polymer rises slowly at the beginning, and approaches

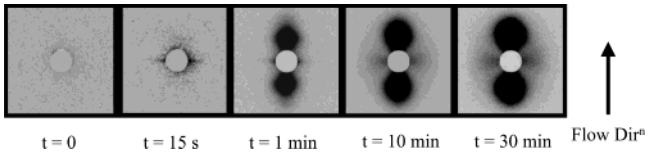

Figure 5. 2D SAXS patterns of the LCB 013 polymer melt before and at selected times after shear (shear rate = 60 s^{-1}, t_s = 0.25 s, T = 140 °C).

Table 2. Mechanical Properties of the LCB-iPP Polymers

sample	flexural modulus (MPa)	yield strength (MPa)	HDT (°C)
LCB 01	1560	36.4	108.5
LCB 05	1790	37.3	117.1
LCB 07	1810	38.4	117.2
LCB 13	1880	38.9	113.6

a plateau value at longer times. In contrast, the LCB-iPP polymer displays an increased viscosity (or strain hardening) at all three strains employed during our tests. The linear iPP polymer (LCB 01) does not show any strain hardening. The experimental extensional viscosity data track the linear viscosity data without showing any hints of an upswing through the break point. Clearly, the LCB-iPP polymers show a significant strain hardening, which in turn indicates pronounced enhancement in melt strength. Strain hardening is a desired feature in processes involving extensional deformation; such as thermoforming, blow molding, foaming, and fiber spinning, etc. This material behavior is also expected to promote the stability of the flow-induced crystallization precursor structure.

Mechanical Properties. The mechanical properties: flexural modulus, tensile yield strength, and heat distortion temperature (HDT), for the LCB-iPP polymers, are shown in Table 2. The LCB-iPP polymers showed significant enhancement in the flexural modulus (upto 20%) and HDT (5−10 °C) compared to the linear iPP polymer (LCB 01). The enhancement in the mechanical properties of the injection molded specimen can be attributed to the development of oriented skin layer. Our optical microscopy studies[28] showed that in the case of the LCB-iPP polymer the thickness of the layer is more than an order of magnitude higher than the linear iPP polymer. The oriented skin layer is typically characterized by the presence of many layers, called "threads', containing row nucleated structures. The core is characterized by spherulites. The formation of row nucleated structures is attributed to the parallel molecular orientation and alignment due to stronger flow conditions near the surface compared to the core. In the LCB-iPP polymers, the orientation and thickness of the oriented skin layer can be related to the molecular architecture of these polymers. Here again, long chain branching in high molecular weight species in these polymers plays a critical role.

In Situ Rheo-SAXS and -WAXD Results. Rheo-SAXS. Figure 5 illustrates a representative series of two-dimensional (2D) in situ SAXS patterns of LCB 13 sample at 140 °C before and after application of step shear (rate = 60 s^{-1}, t_s = 0.25 s). The pattern of the initial amorphous melt (at t = 0) consists of a weak diffuse ring from the isotropic melt, indicative of the absence of any detectable structures and/or preferred orientation. This pattern was observed for all four samples before shear, confirming thermal clearing of memory effects in the polymer melt. The SAXS patterns obtained immediately after shear (at t = 15 s) clearly

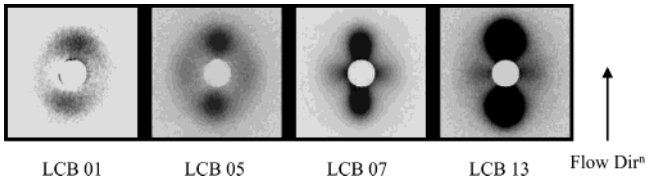

Figure 6. Comparison of 2D SAXS patterns of the four LCB-iPP polymers 30 min after shear (shear rate = 60 s^{-1}, t_s = 0.25 s, T = 140 °C).

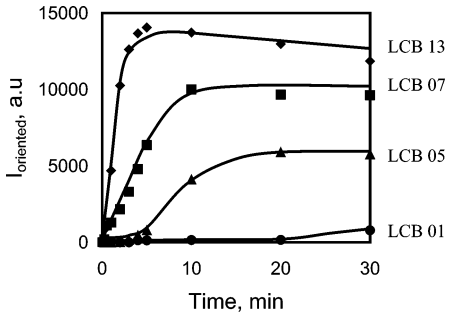

Figure 7. Comparison of the time evolution of SAXS intensity due to oriented crystals ($I_{oriented}$) after shear (shear rate = 60 s^{-1}, t_s = 0.25 s, T = 140 °C) for the LCB-iPP polymers.

show the emergence of an equatorial streak. Subsequent SAXS patterns at t = 1, 10, and 30 min show strong reflections along the equator as well as in the meridian. The flow direction is vertical and is considered the same as the fiber axis. The emergence of equatorial streak is attributed to the formation of oriented structures (microfibrils or shish) parallel to the flow direction and the meridional maxima is attributed to layerlike oriented structures perpendicular to flow direction or kebabs.

Figure 6 compares the SAXS patterns obtained at 140 °C and 30 min after shear for the four chosen LCB-iPP samples. The patterns clearly show that due to the oriented structures both SAXS intensities along the equator and the meridian increase with the branching level. The total SAXS integrated intensity can be deconvoluted into contributions from oriented and unoriented scatterers using the "Halo" method.[52] The total scattered intensity, ($I_{total}[s,\phi]$), from the polymer sample has two components, (1) $I_{unoriented}[s]$, which is due to scattering from the isotropic (unoriented) scatterers including the amorphous melt and background, and (2) $I_{oriented}[s,\phi]$, originated by scattering from the oriented structures. The total scattered intensity can be represented as follows:

$$I_{total}[s,\phi] = I_{unoriented}[s] + I_{oriented}[s,\phi] \qquad (8)$$

where $s = 2 \sin \theta/\lambda$ is the scattering vector, 2θ is the scattering angle, and ϕ is the azimuthal angle. The isotropic component is azimuthal independent (a function of s only), while the scattering arising from the oriented scatterers is azimuthal dependent (function of s and ϕ). The isotropic component of the total intensity, $I_{unoriented}$, was obtained from the Halo method. And, the scattering due to oriented structures, $I_{oriented}$, was calculated as the difference between I_{total} and $I_{oriented}$ (eq 8). Figure 7 shows the time evolution of $I_{oriented}$ for the LCB-iPP polymers. Note here that the intensity values were normalized with respect to the initial value of the intensity due to the amorphous melt and background assuming that the scattering due to oriented structures was zero at t = 0. For LCB 05, LCB 07, and LCB 13 samples, $I_{oriented}$ is seen to rise immediately after application of the shear. However, in the case of linear iPP sample (LCB 01), $I_{oriented}$ rises at a much later time after imposing the shear. Note that the sensitivity of the detector limits the measurement of scattered intensity at the early stages; especially when the emerging crystals concentration is low and/or the size is small. While both unoriented (spherulitic) and oriented crystals grow simultaneously, $I_{oriented}$ (obtained after subtraction of $I_{unoriented}$) is attributed to the oriented crystals growth after cessation of shear. In all the samples, $I_{oriented}$ subsequently reaches a plateau value indicative of complete crystallization at the chosen temperature. The behavior was also verified by the corresponding WAXD patterns. Both SAXS patterns in Figure 6 and $I_{oriented}$ plateau values in Figure 7, show that under identical applied shear conditions, oriented structures fraction is significantly larger in the LCB-iPP polymers than the linear iPP polymer. Note that for LCB 13 sample, $I_{oriented}$ appears to decrease at the later stages. We attribute this behavior to the reorganization of the unoriented and oriented crystals in the melt. In the LCB 13 sample, crystals grow very rapidly after cessation of shear as evidenced by the sudden rise in the SAXS intensity. It is likely that at the later stages, the oriented crystals partly lose the degree of orientation due to the rapid and simultaneous growth of oriented and unoriented crystals.

Lorentz-corrected 1D SAXS intensity profiles (Iq^2 vs q) along the shear direction were extracted from the 2D SAXS images at selected times after shear to follow the change in the intensity distribution of meridional reflections with increasing time. Selected profiles for samples LCB 13 and LCB 07 are shown in Figure 8, parts A and B, respectively. The peak in these profiles corresponds to the meridional maximum, which can be clearly observed at the later stages. From the profiles at the initial stages, the time of emergence of the meridional maximum was estimated as 30 and 60 s for LCB 13 and LCB 07, respectively. This is consistent with the observation that the equatorial streak emerged before the meridional maximum. The spacing between the kebab-like crystals ($L = 2\pi/q$) appears to slightly decrease with time. It probably arises from the ordering process in crystals during crystallization. However, it is our opinion that the change is not very significant. Figure 8C shows the intensity profiles 30 min after shear for all the four samples. The intensity of the meridional maximum is rather weak in LCB 01 sample, due to very low concentration of emerging crystals in the melt. Nevertheless, the values of the long spacing as estimated from the intensity profiles are in the range 230−280 Å for all four samples.

Rheo-WAXD. Nature of the Crystalline Phase in LCB-iPP. The three crystalline forms, α, β, and γ, of isotactic polypropylene have their own distinctive reflections in their WAXD patterns. α-Crystals reflections[49] are indexed as follows, using the wavelength = 1.54 Å: (110) at 2θ = 14.1°, (040) at 16.9°, (130) at 18.5°, (111) at 21.4°, and (−131) at 21.8°. Similarly β-crystals are expected to exhibit the following reflections: (300) at 2θ = 16.1° and (311) at 21.4°. Note that the (311) reflection of the β-form coincides with the (111) reflection of α-crystals; however, the (300) reflection of β-crystals is distinctly separate from all the α-crystal reflections. And thus, it is usually the one that is taken as a marker for β-crystals. The γ-crystals reflections are indexed as follows:[53] (111) at 13.8°, (113) at 15.0°, (115)

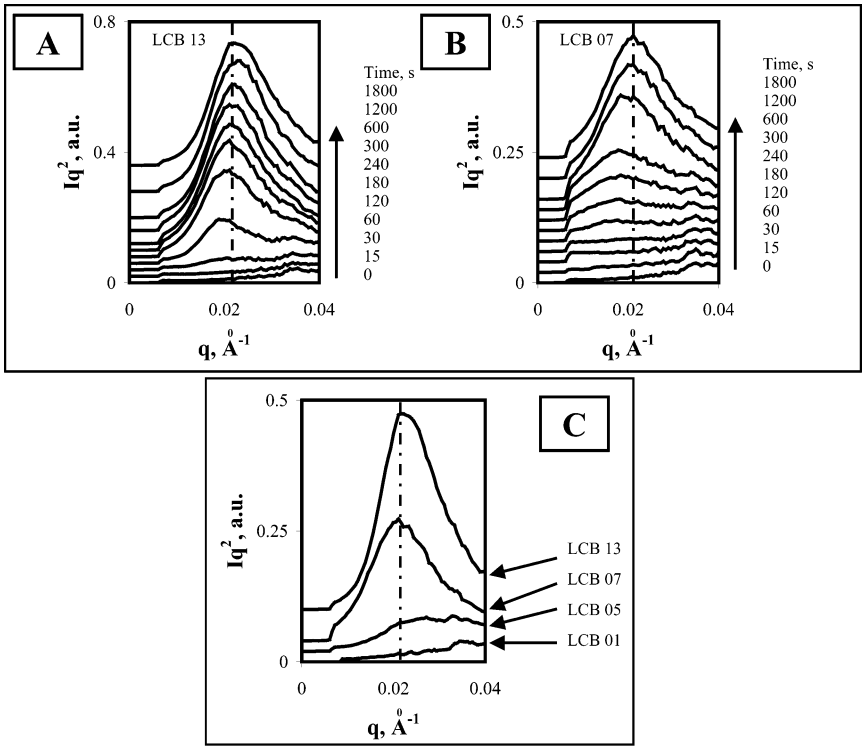

Figure 8. Lorentz-corrected SAXS intensity profiles along the meridian: (A) for LCB 13 at selected times after shear; (B) for LCB 07 at selected times after shear; (C) 30 min after shear (shear rate = 60 s^{-1}, t_s = 0.25 s, T = 140 °C).

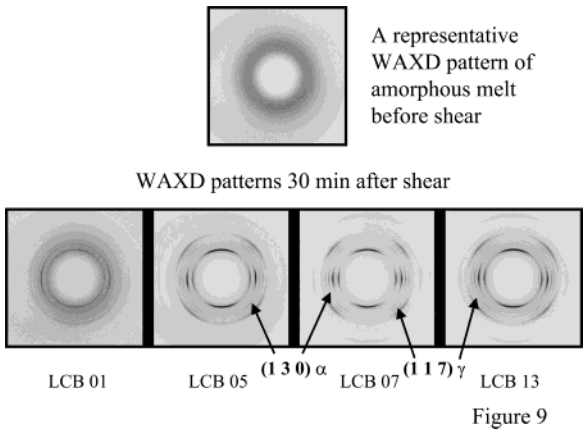

Figure 9. 2D WAXD patterns of the LCB-iPP polymer melts: (a) one representative pattern for all four samples before shear; (b) comparison of the patterns of four LCB-iPP polymers 30 min after shear (shear rate = 60 s^{-1}, t_s = 0.25 s, T = 145 °C).

at 17.2°, (117) at 20.1°, (202) at 21.2°, and (026) at 21.9°. While many reflections of γ-crystals are close and almost overlap with those of α-crystal reflections, the (117) reflection of γ-form is distinctly separated from all the reflections of both α-and β-crystals. The (117) reflection is used as a marker for the γ-phase.

Two-dimensional (2D) WAXD patterns of the LCB-iPP samples at 140 °C, before and 30 min after shear, are shown in Figure 9. Only one representative WAXD pattern before shear (at t = 0) is presented in Figure 9. It shows a diffuse scattering without any crystalline reflections that clearly arises from a completely amorphous polymer melt. A similar pattern was observed before shear for all the four samples studied. In the 2D WAXD patterns, the variation in the intensity of crystal reflections as a function of azimuthal angle is an indication of crystal orientation. When the crystal orientation is random, the intensity of reflections is uniform and circular rings are observed. On the other hand, when the crystals orientation is high, the azimuthal breadths are relatively narrow and arcs or spots are observed. Reflections due to oriented crystals were observed in WAXD patterns immediately after shear by noting intensity arcs along the equator. The intensity of these arcs become stronger with time. In addition, they are superimposed by the uniform intensity ring at later stages due to the growth of unoriented crystals in the melt. Also seen in Figure 9 is that all the samples, including the linear iPP polymer, show both α- and γ-crystal reflections. In the case of LCB-iPP polymers, the azimuthal breadths (in the intensity of α- and γ-crystal reflections) are relatively narrow indicating that the crystal orientation is high. On the other hand, in the linear iPP polymer sample (LCB 01), the α-crystal orientation is relatively weak. Its γ-crystals are mostly isotropic and randomly oriented. Clearly, under identical applied shear conditions, crystal orientation is stronger in LCB-iPP polymers compared to the linear iPP polymer. Note that the β-crystal reflections are not observed in the WAXD patterns of these metallocene-catalyzed LCB-iPP polymers. This is in contrast with the crystallization behavior of Ziegler−Natta iPP (ZN−PP) melts after shear. Our previous study[49] has shown that, under similar flow conditions, in ZN−PP melts a large amount of β-phase is formed.

To determine the time evolution of the crystalline phase, and relative contributions of α and γ-crystals to the total crystalline phase, circularly averaged intensity profiles were extracted from the WAXD patterns. It is noted that for the calculation of crystallinity, the above procedure is prone to error, especially when the WAXD patterns has strong reflection peak near the meridian. In the present case, most of the crystal reflections show strong peaks along the equator (except for the (110) reflection). It is our opinion that even with "Fraser

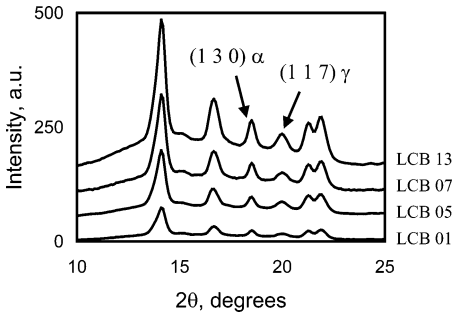

Figure 10. Circularly averaged WAXD intensity profiles at t = 30 min after shear (shear rate = 60 s^{-1}, t_s = 0.25 s, T = 140 °C).

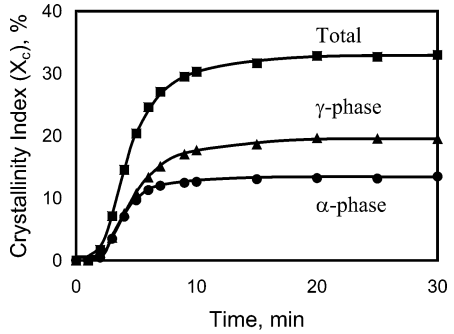

Figure 11. Development of total crystallinity and contributions of α- and γ-crystals to the total crystalline phase in LCB 05 polymer sample after shear (shear rate = 60 s^{-1}, t_s = 0.25 s, T = 140 °C).

correction", the difference in the calculated values of crystallinity may not be significant. However, in the interest of clarity we have chosen to use "crystallinity index" in place of "crystallinity" in this paper. The averaged intensity profiles at 30 min after shear for the LCB-iPP polymers are shown in Figure 10. A standard peak-fit procedure[49] was used to deconvolute the peaks in the WAXD profiles. Each crystal reflection peak position, height and width, and the integrated intensity (peak area) as well as the amorphous background area were obtained from the results of the deconvolution procedure. The percent total crystalline phase in the polymer melt was calculated after subtraction of the area of the amorphous background. The contributions of the α and γ crystals to the total crystalline phase were estimated from relative peak areas of the (130) for α-form and (117) for γ-form reflections.[56] Figure 11 is a representative plot of the nature of the time evolution of the total crystalline phase, and α- and γ-phase components in the LCB-iPP polymers (LCB 05) after shear. Both α- and γ-crystals form in the polymer melt immediately after shear. The volume fractions of α- and γ-phase increases with time due to crystal growth, reaching to a plateau value after some time when the growth process is complete. For the LCB-iPP polymers the plateau value of total crystallinty index (X_c) and relative contributions of α- and γ-phases are presented in Table 3. The plateau value of the total crystallinity index was found to be about 33% in the polymer melt at 140 °C after shear for all samples. The elapsed time after shear to reach the crystalline index plateau value is different for each sample being dependent upon the crystallization kinetics. Clearly, the LCB-iPP polymers crystallize much faster than the linear polymer. It is interesting to note that the amount of γ-phase with respect to the total crystalline phase is found to be as

Table 3. Percent Crystallinity and Crystallization Kinetics of the LCB-iPP Polymers at 140 °C after Shear (Rate = 60 s^{-1}, t_s = 0.25 s)[a]

	crystallinity index, % (plateau values)			crystallization kinetics	
sample	total	α-phase $X_{c\alpha}/f_\alpha$	γ-phase $X_{c\gamma}/f_\gamma$	half-time $t_{1/2}$ (s)	Avrami exponent n
LCB 01	33.1	15.7/0.47	17.4/0.53	2130	3
LCB 05	33.0	13.5/0.41	19.5/0.59	260	2.3
LCB 07	33.1	13.4/0.40	19.7/0.60	85	1.2
LCB 13	32.5	13.7/0.42	18.8/0.58	180[b]	1.3

[a] Key: $X_{c\alpha}$, crystallinity index of the α-phase; $X_{c\gamma}$, crystallinity index of the γ-phase; f_α, fraction of the α-phase; f_γ, fraction of the γ-phase. [b] Note that the number-average molecular weight (M_n) for this resin is higher than the other three resins.

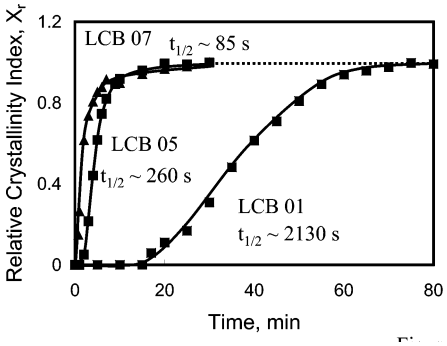

Figure 12. Half-time of crystallization for LCB 01, 05, and 07 polymers after shear (rate = 60 s^{-1}, t_s = 0.25 s, T = 140 °C).

high as 58−60% in the LCB-iPP polymers. It is about 53% in the linear iPP polymer. At present, we do not think that the differences are significant. For the present analysis and discussion the relative contributions of α- and γ-phases are considered to be the same for all samples and independent of the branching level. The factors, such as chain microstructure, chain defects, and comonomers, etc., that may profoundly affect the formation of the γ-phase in iPP polymers is presented in the discussion section.

Crystallization Kinetics under Shear. The half-time of crystallization ($t_{1/2}$) was determined from the plot of relative crystallinity index (X_r), as defined in eq 9, vs time.

$$X_r = \frac{X_c(t)}{X_c(\infty)} \tag{9}$$

where X_r is the relative crystallinity index, $X_c(t)$ is the total crystallinity index at time t, and $X_c(\infty)$ is the steady-state value (plateau value) of the total crystallinity index. The half-time of crystallization was determined as the time at which the relative crystallinity index reaches a value of 0.5. Figure 11 shows the development of the relative crystallinity index with time at 140 °C after shear for LCB 01, 05, and 07. Since LCB 01, 05, and 07 samples have comparable number-average molecular weight values, their results can be used to evaluate the effects of branching on the crystallization kinetics under flow. However, following the above procedure, the $t_{1/2}$ value for LCB 13 sample was also determined; all calculated values of $t_{1/2}$ appear in Table 3.

The effects of LCB on the melt crystallization kinetics under shear can be clearly seen in Figure 12. The LCB-iPP polymers crystallize much faster than the linear

polymer. The $t_{1/2}$ value for the LCB-iPP polymers (LCB 05 and LCB 07) is about 1 order of magnitude smaller than that for the linear iPP polymer. The increase in the kinetics is generally attributed to an increase in the crystal nuclei due to orientation of the polymer molecules and the formation of a stable crystallization precursor structure in the sheared melt. Thus, due to their stronger orientation (as evidenced by in situ SAXS and WAXD results in Figures 6 and 8) in LCB-iPP polymers compared to the linear iPP polymer, the effect in crystallization kinetics in the branched polymers is very much pronounced.

It should be noted here that the crystallization half times can be estimated from the SAXS intensity profiles in Figure 7. The $t_{1/2}$ values, the time to reach 50% of the plateau value of I_{oriented}, are 1420, 490 240, and 75 s for LCB 01, 05, 07, and 13, respectively. The corresponding values from WAXD are 2130, 260, 85, and 180 s for LCB 01, 05, 07, and 13, respectively. In WAXD, some samples show shorter times, while the others show longer times than SAXS. This apparent inconsistency may arise due to the fundamental differences between SAXS and WAXD. SAXS intensity arises from the difference in the density of scatterer (such as, crystal, mesophase, impurities, dust, etc.) and the surrounding medium (such as amorphous melt), while WAXD intensity arises directly from the crystalline phase. SAXS is much more sensitive than WAXD and is very useful in following structure development in the polymer melt, especially at the early stages of crystallization, which is clear from the rapid rise in SAXS intensity in Figure 7. However, we believe that crystallization half-times from WAXD data represent the crystallization kinetics more accurately than those from SAXS.

The Avrami model, expressed in eqs 10 and 11, was used to obtain quantitative information about crystal growth geometry.

$$1 - X_r = e^{-kt^n} \tag{10}$$

$$\ln[-\ln(1 - X_r)] = \ln(k) + n \ln(t) \tag{11}$$

where k and n are the two Avrami parameters usually referred to as the bulk crystallization constant and Avrami exponent, respectively. The Avrami crystallization constant (k) is dependent on the shape (rod/disk/sphere) of the growing crystalline entities and the amount and type of nucleation (thermal or athermal). The exponent (n) is dependent upon the nucleation type and growth geometry but not on the amount of nucleation. In athermal type of nucleation; for $n \sim 1$, a linear or rodlike crystal growth geometry is expected; for $n \sim 2$, it is expected to be disklike; and for $n \sim 3$, it is spherelike. In polymer crystallization from an entangled melt, noninteger values of n are often obtained, indicative of an overlap of different crystal growth geometries.

The Avrami plot, $\ln[-\ln(1 - X_r)]$ vs $\ln(t)$, for LCB 01, LCB 05, and LCB 07, samples is shown in Figure 13. Although there are significant deviations from the model at the later stages of crystallization, the value of Avrami exponent can be determined from the slope of the fitted line to the data at the initial stages. A value of $n \sim 3$ was obtained for the linear iPP polymer (LCB 01) which is indicative of the unoriented spherulitic crystal growth in polymer melt after shear; on the other hand, values of $n \sim 2.8$ and 1.8 are obtained for the branched LCB 05 and LCB 07 polymers, respectively. A lower value of n (<3) indicates a rod/disklike crystal growth geometry. These results are consistent with in situ SAXS images in Figures 5 and 6.

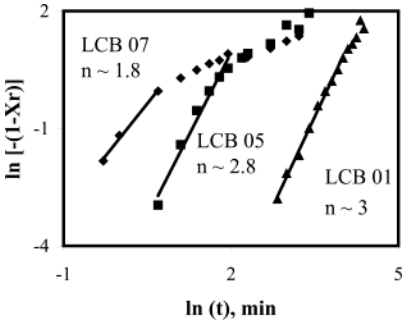

Figure 13. Avrami plot of the crystallization data for LCB 01, 05, and 07 polymers at 140 °C after shear (rate = 60 s^{-1}, t_s = 0.25 s).

Table 4. Longest Relaxation Time of the LCB-iPP Polymers at 180 °C (from SAOS Data)[a]

sample	λ (s)
LCB 01	3.2
LCB 05	54.3
LCB 07	91.2
LCB 13	818

[a] λ is the longest relaxation time.

Discussion

Characteristic Properties of the Novel LCB-iPP Polymers. The results of various characterization techniques have clearly shown that the long chain branched LCB-iPP polymers, in which LCB was introduced via in situ polymerization of propylene and a diene monomer using the metallocene catalyst technology, exhibit many property changes compared to the linear iPP polymer. The notable property enhancemants include; high melt strength, high tensile strength, and high heat distortion temperatures. These enhancements are desirable in various applications where conventional linear iPPs have not succeeded due to their inherent structural limitations. These properties improvements are attibuted to the unique chain architecture of the LCB-iPP polymers: highly branched species residing mainly at the high molecular weight species in the molecular weight distribution, as evidenced by the GPC−MALLS analysis.

The unique molecular architecture of the LCB-iPP polymers also play a critical role in the nature and habits of formation, α- and γ-forms, in addition to orientation of the crystalline phases and melt crystallization kinetics that is exacerbated in flow fields, a topic discussed below in detail.

Effects of Long Chain Branching. Relaxation Time and Flow-Induced Crystallization. At a given temperature, the relaxation time increases with the branching level,[54] which is evidenced by the relaxation spectra of the LCB-iPP samples in Figure 3. Note that, even though the data of Figure 3 was obtained at a temperature of 180 °C and the X-ray experiments were done at 140 °C; the trend in the differences in relaxation behavior of the LCB-iPP samples should be similar at lower melt temperatures (presuming that the sample does not crystallize fast enough to influence the relaxation spectrum). The numerical values of the longest relaxation times are presented in Table 4. The significant differences in the longest relaxation time of the highly branched and/or high molecular weight species

between the four polymer samples are clearly noted. Thus, the highly branched molecules take a longer time for relaxation from orientation. In view of this, it is conjectured that the oriented segments of highly branched species take part in the formation of precursors of primary nuclei for crystallization of extended chain crystals. Our previous study[55] has shown that in iPP melts, even a small amount of the shishlike extended chain crystals induces nucleation and growth of a large amount of kebablike crystal lamellae. The in situ SAXS and WAXD observations are consistent with this scenario. The SAXS results (Figures 5−8) and WAXD results (Figure 9) show that the fractions of highly oriented crystals are significantly higher in the branched polymers (LCB 05, 07, and 13) as compared to the linear iPP polymer (LCB 01).

Crystallization Kinetics and Avrami Exponent. The crystallization kinetics in the branched polymers compared to the linear iPP polymer increased by more than an order of magnitude (Figure 12 and Table 3), which can be related to the formation of higher number of linear primary nuclei and their stability for a longer duration after cessation of flow. The analysis of crystallinity data from WAXD using Avrami model indicate a rod- and disklike crystal growth geometry in the branched samples and a spherulitic crystal growth geometry in the linear iPP polymer. These results are consistent with the hypothesis that a large amount of linear nuclei for crystallization of extended chain crystals (rodlike) form immediately after shear and that highly branched molecules are more likely to form these nuclei due to their longer relaxation times. The chain-folded crystals grow radially outward from many nucleation sites along the length of nuclei. It is conceivable, if the nuclei density is very high (LCB 07), then the interactions between the lamellar growth are strong, resulting in a rodlike (1D) growth mechanism. If the nuclei density is intermediate (LCB 05) then a disklike (2D) growth prevails.

γ-Phase in the LCB-iPP Polymers. The formation of the γ-phase in the LCB-iPP polymers could be related to the applied shear and/or the oriented α-crystals. To evaluate this possibility, the following analysis was carried out. Final total crystllinity, plateau values and relative contributions of α- and γ-phase obtained from the WAXD data (Table 3) are about the same for all samples including that of the linear iPP polymer. In addition, the inception time of α- and γ-phase is independent of each other. Both phases form immediately after shear, as evident from their growth curves shown in Figure 11. These results indicate that the formation of γ-phase in the LCB polymers is *not* dependent on the applied flow conditions. It is probably related to the chain architectural details.

It has been shown that in the iPP materials prepared using the metallocene catalyst technology[56,57] a mixture of α- and γ-phase forms. The structural model of the γ-crystals is characterized by a nonparallel arrangement of the chains within the unit cell.[53] The content of the γ-phase is favored by the presence of defects in iPP chain that could be due to either stereo, regio, and/or counits. In i-PP polymers with regio defects concentration of greater than 4.4%, 100% γ-phase has been shown to develop. Similarly, in certain cases, only with 0.4% regio defects, 10% γ-phase has been obtained. The γ phase in the LCB-iPP polymers is attributed to the level of chain defects more so than the LCB introduced by diene.

Conclusions

1. The characteristic properties of a new class of the long chain branched isotactic polypropylene (LCB-iPP) polymers, in which LCB was introduced via in situ polymerization of propylene and a miniscule amount of a diene monomer using metallocene catalyst technology, exhibit a rather intriguing property profile. For example, compared to the linear iPP polymer, they exhibit improved melt strength and mechanical properties such as flexural modulus and tensile yield strength, etc. These polymers have a unique molecular architecture. Generally, highly branched species in them reside at molecules in the high molecular weight tail end of the molecular weight distribution.

2. Upon application of shear (rate = 60 s^{-1}, $t_s = 0.25$ s, $T = 140$ °C), the oriented crystalline fractions are substantially higher in the LCB-iPP polymers than linear iPP polymer. Also, their crystallization kinetics is improved by more than an order of magnitude. The values of the Avrami exponent ($n \sim 1.8$ to 2.8) indicate a rod or disklike crystal growth geometry in the LCB-iPP polymers, probably resulting from the flow-induced nucleation density. Such obervations are consistent with the in situ SAXS and WAXD patterns.

3. The LCB-iPP polymers crystallize in both the α- and γ-forms. The formation of γ-phase is promoted, perhaps mainly due to the regio defects introduced during polymerization by the metallocene catalyst technology employed.

4. The strong crystal orientation and improved crystallization kinetics in flow are attributed to the unique molecular architecture of the LCB-iPP polymers and its related effect on their broadened and complex relaxation behavior.

Acknowledgment. We wish to acknowledge the assistance of Drs. Fengji Yeh and Dufei Fang for synchrotron SAXS and WAXD experimental setup. The financial support of this work was provided by the NSF (DMR-0098104) and ExxonMobil Co.

References and Notes

(1) Keller, A.; Kolnaar, H. W. *Mater. Sci. Technol.* **1997**, *18*, 189.
(2) Eder, G.; Janeschitz-Kriegl, H. *Mater. Sci. Technol.* **1997**, *18*, 268.
(3) Wunderlich, B. *Macromolecular Physics*; Academic: New York, 1973; Vol. 2.
(4) Keller, A.; Hikosaka, M.; Rastogi, S. *Phys. Sci.* **1996**, *T66*, 243.
(5) Keller, A.; Hikosaka, M.; Rastogi, S.; Toda, A.; Barham, P. J.; Goldbeck-Wood, G. *J. Mater. Sci.* **1994**, *29*, 2579.
(6) Keller, A.; Cheng, S. Z. D. *Polymer* **1998**, *39*, 4461.
(7) Pennings, A. J.; Van der mark, J. M. A.; Booij, H. C. *Kolloid. Z. Z. Polym.* **1970**, *236*, 99.
(8) Mackley, M. R.; Keller, A. *Polymer* **1973**, *14*, 16.
(9) Pope, D. P.; Keller, A. *Colloid Polym. Sci.* **1978**, *256*, 751.
(10) Miles, M. J.; Keller, A. *Polymer* **1980**, *21*, 1295.
(11) Kalay, G.; Bevis, M. J. *J. Polym. Sci., Polym. Phys.* **1997**, *35*, 265.
(12) Wilkinson, A. N.; Ryan, A. J. *Polymer Processing and Structure Development*; Kluwer: Dordrecht, The Netherlands, 1998.
(13) Varga, J. *J. Mater. Sci.* **1992**, *27*, 2557.
(14) Varga, J.; Karger-Kocsis, J. *J. Polym. Sci., Part B, Polym. Phys.* **1996**, *34*, 657.
(15) Vleeshouwers, S.; Meijer, H. E. H. *Rheol. Acta* **1996**, *35*, 391.
(16) White, H. M.; Bassett, D. C. *Polymer* **1997**, *38*, 5515.
(17) Goschel, U.; Swartjes, F. H. M.; Peters, G.. W. M.; Meijer, H. E. H. *Polymer* **2000**, *41*, 1541.

(18) Devaux, N.; Monasse, B.; Haudin, J. M.; Vermant, J.; Moldenaers, P.; Andre, J. M.; Ernst, B. *Proceedings of the International Conference on Flow Induced Crystallization of Polymers*, Salerno, Italy, 14−17, 2001; p 31.
(19) Jerschow, P.; Janeschitz-Kriegl, H. *Int. Polym. Process.* **1997**, *12(1)*, 72.
(20) Eder, G.; Janeschitz-Kriegl, H.; Liedauer, S. *Prog. Polym. Sci.* **1990**, *15*, 629.
(21) Lohse, D. J.; Milner, S. T.; Fetters, L. J.; Xenidou, M.; Hadjicristidis, N.; Mendelson, R. A.; Garcia-Franco, C. A.; Lyon, M. K. *Macromolecules* **2002**, *35*, 3066.
(22) Vega, J. F.; Muñoz-Escalona, A.; Santamaria, A.; Muñoz, M. E.; Lafuente, P. *Macromolecules* **1996**, *29*, 960.
(23) Malmberg, A.; Kokko, E.; Lehmus, P.; Logren, B.; Seppala, J. V. *Macromolecules* **1998**, *31*, 8448.
(24) Markel, E. J.; Weng, W. Q.; Peacock, A. J.; Dekmezian, A. H. *Macromolecules* **2000**, *33*, 8541.
(25) Weng, W.; Hu, W.; Dekmezian, A. H.; Ruff, C. J. *Macromolecules* **2002**, *35*, 3838.
(26) Weng, W.; Marke, E. J.; Dekmezian, A. H. *Macromol. Rapid Commun.* **2000**, *21*, 103.
(27) Weng, W.; Marke, E. J.; Dekmezian, A. H. *Macromol. Rapid Commun.* **2001**, *22*, 1488.
(28) Agarwal, P. K.; Weng, W.; Mehta, A. K.; Dekmezian, A. H.; Chang, M.; Chudgar, R. K.; Davey, C. R.; Lin, C. Y.; Chen, M. C.; Richeson, G. C. U.S. Patent No. US 2002/0013440 A1, Jan 31, 2002.
(29) Strobl, G. *Eur. Polym. J.* **2000**, *E3*, 165.
(30) Lotz, B. *Eur. Polym. J.* **2000**, *E3*, 185.
(31) Kumaraswamy, G.; Kornfield, J. A.; Yeh, F.; Hsiao, B. S. *Macromolecules* **2002**, *35*, 1762.
(32) Seki, M.; Thurman, D. W.; Oberhauser, J. P.; Kornfield, J. A. *Macromolecules* **2002**, *35*, 2583.
(33) Mitchell, G. R.; Holt, J. J.; Thornley, S. A.; Chai, C. K. *Proceedings of the Interantional Conference on Flow Induced Crystallization of Polymers*; Salerno, Italy, 14−17, 2001; p 15.
(34) Ryan, J.; Terrill, N. J.; Fairclough, J. P. A. In *Scattering of Polymers*; Cebe, P., Hsiao, B. S., Lohse, D. J., Eds.; ACS Symposium Series 739; Oxford: Washington D. C. 2000; p 201.
(35) Terrill, N. J.; Fairclough, J. P. A.; Towns-Andrews, E.; Komanschek, B. U.; Young, R. J.; Ryan, A. J. *Polymer* **1998**, *39*, 2381.
(36) Liu, C.; Muthukumar, M. *J. Chem. Phys.* **1998**, *109*, 2536.
(37) Muthukumar, M. *Eur. Phys. J. E: Soft Matter* **2000**, *3* (2), 199.
(38) Wang, Z. G.; Hsiao, B. S.; Sirota, E. B.; Srinivas, S. *Polymer* **2000**, *41*, 8825.
(39) Cheng, S. Z. D.; Li, C. Y.; Zhu, L. *Eur. Phys. J. E: Soft Matter* **2000**, *3* (2), 195.
(40) Lieberwirth, I.; Loos, J.; Petermann, J.; Keller, A. *J. Polym. Sci., Part B, Polym. Phys.* **2000**, *38*, 1183.
(41) Pennings, A. J.; Kiel, A. M. *Kolloid Z. Z. Polym.* **1965**, *205*, 160.
(42) Somani, R. H.; Yang, L.; Hsiao, B. S. *Physica A* **2002**, *304*, 145.
(43) Somani, R. H.; Nogales, A.; Srinivas, S.; Fruitwala, H.; Tsou, A. H.; Hsiao, B. S. *Proceedings of the International Conference on Flow Induced Crystallization of Polymers*; Salerno, Italy, 14−17, 2001; p 21.
(44) Somani, R. H.; Bruger, C.; Hsiao, B. S.; Stein, R. S. *Proceedings of ACS Division of Polymeric Materials: Science and Engineering*, Chicago, August 26−30, 2001; American Chemical Society: Washington, DC, Vol. 85, p 429.
(45) Pogodina, N. V.; Lavrenko, V. P.; Winter, H. H.; Srinivas, S. *Polymer* **2001**, *42*, 9031.
(46) Alfonso, G. C.; Azzurri, F. *Proceedings of the International Conference on Flow Induced Crystallization of Polymers*; Salerno, Italy, 14−17, 2001; p 27.
(47) Somani, R. H.; Hsiao, B. S.; Nogales, A.; Srinivas, S. Tsou, A. H.; Sics, I.; Balta-Calleja, F.; Ezquerra, T. A. *Macromolecules* **2000**, *33*, 9385.
(48) Nogales, A.; Hsiao, B. S.; Somani, R. H.; Srinivas, S. Tsou, A. H.; Balta-Calleja, F.; Ezquerra, T. A. *Polymer* **2000**, *42*, 5247.
(49) Somani, R. H.; Hsiao, B. S.; Nogales, A.; Srinivas, S. Tsou, A. H.; Balta-Calleja, F.; Ezquerra, T. A. *Macromolecules* **2001**, *34*, 5902.
(50) Baumgaertel, N.; Winter, H. H. *Rheol. Acta* **1989**, *28*, 511.
(51) Meissner, J. *Rheol. Acta* **1969**, *8*, 78.
(52) Ran, S.; Zong, X.; Fang, D.; Hsiao, B. S.; Chu, B.; Ross, R. *J. Appl. Crystallogr.* **2000**, *33*, 1031.
(53) Auriemma, F.; Rosa, C. D.; Boscato, T.; Corradini, P. *Macromolecules* **2001**, *34*, 4815.
(54) Ferry, J. D. *Viscoelastic Properties of Polymers*, 2nd ed.; Wiley: New York, 1970.
(55) Somani, R. H.; Yang, L.; Hsiao, B. S.; Agarwal, P.; Fruitwala, H.; Tsou, A. H. *Macromolecules*, submitted for publication.
(56) Perez, E.; Zucchi, D.; Sacchi, M. C.; Forlini, F.; Bello, A. *Polymer* **1999**, *40*, 675.
(57) Foresta, T.; Piccarola, S.; Goldbeck-Wood, G. *Polymer* **2001**, *42*, 1167.

MA034154L